Electron-Yield Enhancement in a Laser-Wakefield Accelerator Driven by Asymmetric Laser Pulses

W. P. Leemans, P. Catravas, E. Esarey, C. G. R. Geddes, C. Toth, R. Trines,* C. B. Schroeder, B. A. Shadwick, J. van Tilborg,* and J. Faure

Lawrence Berkeley National Laboratory, University of California, Berkeley, California 94720

(Received 1 February 2002; published 8 October 2002)

The effect of asymmetric laser pulses on electron yield from a laser wakefield accelerator has been experimentally studied using $> 10^{19}$ cm^{-3} plasmas and a 10 TW, > 45 fs, Ti:Al_2O_3 laser. The laser pulse shape was controlled through nonlinear chirp with a grating pair compressor. Pulses (76 fs FWHM) with a steep rise and positive chirp were found to significantly enhance the electron yield compared to pulses with a gentle rise and negative chirp. Theory and simulation show that fast rising pulses can generate larger amplitude wakes that seed the growth of the self-modulation instability, and that frequency chirp is of minimal importance for the experimental parameters.

DOI: 10.1103/PhysRevLett.89.174802 PACS numbers: 41.75.Jv, 41.75.Ht, 42.65.Re, 52.38.–r

Controlling and optimizing the coupling of laser light to plasma waves is important in numerous applications. Laser-plasma accelerators, which have been proposed as compact next-generation accelerators, rely on laser excitation of large amplitude plasma waves (with 10–100 GV/m fields) for trapping and acceleration of particles [1]. In laser fusion applications, excitation of plasma waves through Raman and/or Brillouin instabilities [2] can cause poor coupling of laser beams onto targets. The use of laser bandwidth, temporal coherence, frequency chirp, and/or pulse shaping have been proposed as methods for controlling these instabilities [3].

Recent 2D particle-in-cell (PIC) simulations [4] were reported in which a linearly chirped laser pulse either suppressed or enhanced the growth of the Raman forward scattering (RFS) instability in the self-modulated laser wakefield accelerator (SM-LWFA) [1,5–9], depending on the sign of the chirp. These simulations were done for symmetric temporal laser envelopes with a large linear chirp [laser bandwidth (FWHM) of 24% on a 120 fs laser pulse]. This is almost an order of magnitude beyond that produced by typical lasers. Experiments have studied the dynamics of RFS using picosecond linearly chirped pulses [9] but found no dependence on the sign of the chirp for laser intensities $\sim 2 \times 10^{17}$ W/cm^2.

The effect of laser pulse shape on plasma wave growth has also been studied theoretically [10,11]. Triangular pulses with a fast rise and slow fall time (compared to the plasma period) have been shown to be more desirable for laser-plasma accelerators, in contrast to those with a slow rise and a fast fall. Whereas, in principle, the plasma wave amplitude *behind* the pulse is very similar for both types of pulses, the fast rise time pulses generate significantly larger wakes *within* the pulse, which can seed violent instabilities. This can disrupt pulse propagation [11] but can also, as shown below, lead to enhanced particle trapping. Such pulses can be generated by chirped-pulse amplification (CPA) lasers [12].

In this Letter, we present the first experimental observations of enhanced acceleration of background electrons in a laser wakefield accelerator by using nonlinearly chirped laser pulses from a 10 Hz, Ti:Al_2O_3, CPA based laser system [8]. The dominant effect of the nonlinear chirp is to cause pulse shape asymmetries with fast rises, which are more unstable to self-modulation and RFS, resulting in larger electron yield. Pulse shaping is found to be more effective than the use of linear chirp in controlling plasma instabilities and in optimizing the performance of laser-plasma devices.

Low energy pulses (laser wavelength $\lambda \simeq 0.8$ μm) from a laser oscillator were first temporally stretched, amplified to 1 J/pulse level and then compressed using a grating based optical compressor (installed in a vacuum chamber) to pulse widths as short as 45 fs. The compressor setting yielding the minimum pulse duration at the gas jet is referred to as the compressor zero. Following compression, the laser beam was focused to a size $w = 6$ μm (Rayleigh length $Z_R \simeq 141$ μm) with a 30 cm focal length ($F/4$) off-axis parabola onto a pulsed gas jet. The vacuum focus location with respect to the gas jet was established as the center of the dumbbell shaped plasma, produced by laser ionization in a <0.5 Torr N_2 backfilled vacuum chamber. The peak power P of the laser was varied using both the pulse duration and laser energy. For the results in this Letter, at optimum compression [full-width-half-maximum (FWHM) duration $\tau_{\mathrm{FWHM}} = 55$ fs], $P \simeq 8.3$ TW, resulting in a peak intensity $I = 2P/\pi w^2 \simeq 1.5 \times 10^{19}$ W/cm^2 and a normalized laser strength $a_0 \approx 8.6 \times 10^{-10} \lambda[\mu\mathrm{m}] I^{1/2}[\mathrm{W/cm^2}] \simeq 2.6$. After the interaction region, the spectral properties were measured using an imaging spectrometer (0.27 m focal length) with a 100 groove/mm grating and a 16 bit charged coupled device (CCD). The laser pulse spectral bandwidth was typically 21–22 nm (FWHM), or $\Delta\omega/\omega_0 \simeq 2.6\%$. The total charge per bunch and spatial profile of the electron beam were measured using an

 © 2002 The American Physical Society

integrating current transformer and phosphor screen imaged onto a 16 bit CCD camera, respectively.

The laser pulse duration, chirp, and envelope characteristics were varied by scanning the compressor grating separation. The laser pulse duration was measured with a single shot autocorrelator (SSA), located outside the vacuum chamber. Temporally resolved spectra of the laser were measured using a frequency resolved optical gating (FROG) system, allowing pulse shape reconstruction. Shapes for positively and negatively chirped pulses with $\tau_{\mathrm{FWHM}} = 76$ fs are shown in Fig. 1. As can be seen, incomplete compensation of accumulated phase nonlinearities with respect to frequency from propagation through the laser system (including the compressor) [13] resulted in positively (negatively) chirped pulses having a fast (slow) rise time. The experimental temporal intensity profiles can be well fitted to a skewed Gaussian of the form $I(t) = I_0 \exp\{[-t^2/(2\tau^2)][1 + bt/(t^2 + \tau^2)^{1/2}]^{-1}\}$, where $|b| < 1$ is the skew parameter, τ is the duration, and I_0 is the peak intensity. In principle, positively chirped pulses can also be generated with slow rise and fast fall times through different compressor tuning.

The forward scattered laser light and electron yield versus relative compressor separation are shown in Figs. 2 and 3, respectively. Typical plasma profiles had peak density in excess of 3×10^{19} cm^{-3} over 700 μm, with a 500 μm ramp from vacuum on either side, as measured interferometrically. The minimum power at which electrons were observed was ~0.9 TW (pulse duration ~500 fs), which is comparable to the critical power for relativistic self-focusing $P_c = 17(\lambda_p/\lambda)^2$ GW [14] for $n_e \simeq 10^{19}$ cm^{-3}. When electrons were produced, spectra showed a clear redshifted sideband, which is attributed to RFS (see Fig. 2). The transmitted laser spectra (Fig. 2), for laser pulses $\gtrsim 170$ fs, indicated that a substantial portion of the laser pulse was blueshifted, on both sides of the compressor zero. At the beam waist and compressor zero, the laser intensity exceeds the appearance intensity of He^{++} by > 100 times and, hence, only the front of the laser pulse undergoes blueshifting. In the absence of relativistic self-focusing, however, as is the case in the density ramps of the jet profile below 10^{19} cm^{-3}, diffraction causes the intensity to reduce and a significant part of the laser pulse can be blueshifted. As soon as the laser power exceeds P_c in the low density regions of the jet, the amount of laser energy that undergoes ionization blueshifting is drastically reduced.

The dependence of electron yield on focal position within the plasma density profile was examined. Two cases are shown in Fig. 3. In case 1, the laser was focused on the upstream edge (low density ~2×10^{18} cm^{-3}) of the gas jet. In case 2, the laser was focused into the jet at a density around 3×10^{19} cm^{-3}. For case 2, the peak plasma density was 25% lower, which is a small correction compared to the difference between the densities at the two focal locations.

For case 1, the maximum electron yield did not occur for the shortest laser pulse duration and was found to be larger for steep pulses (positive chirp) by about a factor 2 compared to gentle pulses (negative chirp). In some runs, order of magnitude asymmetries have been observed in the electron data. For case 2, significantly less asymmetry was seen, and the yield was found to peak close to the compressor zero. Although the peak yield is nearly equal in the two cases, focusing on the gas jet edge produces significantly larger amounts of high energy electrons as previously shown [8].

To correctly interpret the data, it is essential to establish the proper compressor zero. Group velocity dispersion

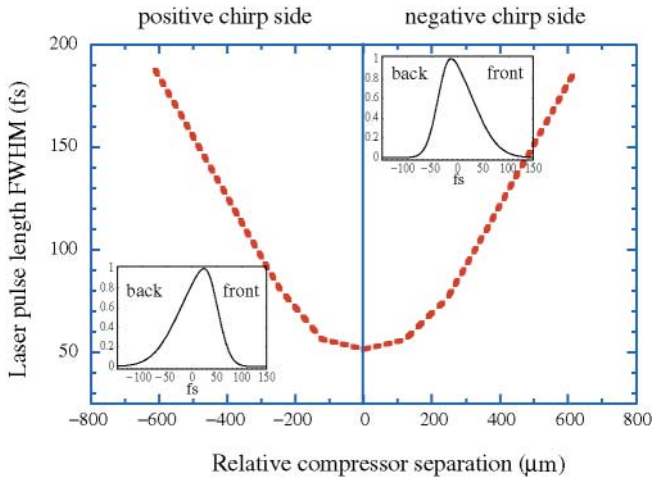

FIG. 1 (color). Pulse duration from SSA (dashed line) vs compressor setting. The insets show the laser pulse envelope $(I(t)/I_0)$ at two relative compressor separations corresponding to positively and negatively skewed pulses ($b = \pm 0.6$) of duration ($\tau_{\mathrm{FWHM}} = 76$ fs).

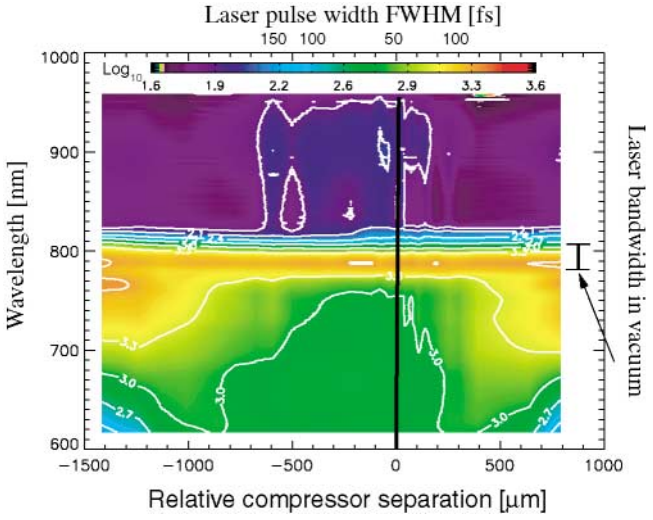

FIG. 2 (color). Forward laser spectra vs compressor setting. The energy was ~460 mJ/pulse and the duration ≥ 50 fs. The laser was focused on the gas jet upstream edge.

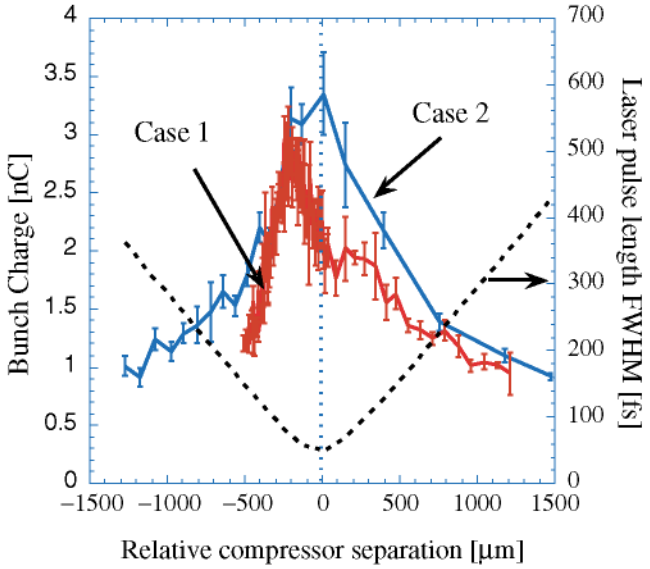

FIG. 3 (color). Electron yield for cases 1 and 2 and pulse duration (dashed line) vs compressor setting. Clear asymmetry in electron yield is observed vs compressor setting for case 1. The energy was ~460 mJ/pulse and the duration ≥ 50 fs.

(GVD) in windows and optical elements affects the pulse duration at the detector. This results in a "false" determination of the optimum grating setting to reach the shortest pulse length at the gas jet. We relied on two "direct" methods that use ionization blueshifting and measurement of the upstream location of the plasma edge.

Ionization blueshifting [15] causes a change in local frequency $\omega(\zeta, z)$ that can be estimated from [16] $\omega^2(\zeta, z) = \omega_0^2 - \int_0^z dz \partial_\zeta \omega_p^2(\zeta, z)$, where $\zeta = z - ct$, z is the propagation distance, ω_0 is the initial laser frequency, and ω_p is the plasma frequency. This model predicts that, at optimum compression, the shortest laser pulse undergoes the largest amount of blueshifting. Rate equations using two-step ionization of He were solved using an ionization rate given by the Keldysh tunneling model, and the experimental gas density profile was used as input. Good agreement between measured and calculated blueshifting was obtained, justifying the use of blueshifting to determine the compressor zero.

As an independent second method for determining the compressor zero, plasma interferograms were analyzed to determine the location of the upstream plasma edge and its dependence on pulse length for constant laser fluence (J/cm^2). The intensity contour at which the ionization threshold is first exceeded moves upstream from the waist as the maximum laser intensity increases. The amount of longitudinal shifting of the location of the plasma edge was overall in good agreement (less than 10% of Z_R deviation) with predictions based on Gaussian isointensity contours [17]. The compressor zero location determined by blueshift and plasma edge measurements were indistinguishable, and both were consistent with the SSA measurement corrected for material GVD.

Several possible mechanisms have been investigated to explain the asymmetry in yield with compressor setting. Growth of RFS including chirp effects was studied analytically [18]. Chirp enhanced RFS could lead to larger particle trapping through interplay with Raman backscatter [19]. The asymptotic growth of the RFS space charge potential $\delta\phi$ can be modeled as $\delta\phi \sim \delta\phi_0 \exp N_{\mathrm{RFS}}$, where $\delta\phi_0$ is the initial seed and N_{RFS} is the number of e-foldings. Using 1D cold fluid theory, we find $N_{\mathrm{RFS}} \simeq 2\Gamma(|\zeta|t/c)^{1/2}$, where $\Gamma = \Gamma_R(1 - \Delta\omega|\zeta|/\omega_0 L)^{1/2}$ is the chirp modified growth rate, $\Gamma_R = \omega_p^2|a_0|/(\sqrt{8}\gamma_\perp\omega)$ is the usual RFS growth rate [20,21], t is the propagation time, and a flattop laser profile $a(\zeta) = a_0$ for $\zeta \in [-L, 0]$ with a local frequency given by $\omega = \omega_0 + \Delta\omega\zeta/L$ was assumed. This indicates that RFS growth is increased by a positive chirp ($\Delta\omega/\omega_0 < 0$) everywhere throughout the pulse. In the standard description for RFS, the growth of laser intensity modulations is caused by local enhancement of axial energy transport due to plasma wave density perturbations [22]. Positive chirp increases this axial transport [4] leading to larger growth, larger accelerating fields, and a more rapid onset of particle trapping. Growth enhancement, however, is small compared to the experimental observations; i.e., in 1D theory a few percent chirp leads to a change in growth on the order of a few percent. This is in agreement with results of 1D PIC simulations using the code XOOPIC [23].

The dominant cause for the asymmetry of the electron yield with chirp was found to be the dependence of the laser pulse shape on chirp, as shown in Fig. 1. Using the experimental laser pulse shape, the plasma response was calculated using the 1D nonlinear fluid equations [1].

Figure 4(a) shows the plasma wave potential $\delta\phi$ ponderomotively excited by the positive $a_+(\zeta)$ and negative $a_-(\zeta)$ skewed laser pulse shapes with $\tau_{\mathrm{FWHM}} = 76$ fs. A larger wake is excited within the laser pulse for the positive compared to the negative skew case. RFS is seeded by the density perturbations which contain Fourier components at the relativistic plasma frequency ω_p. Figure 4(b) shows the ratio of the Fourier components (evaluated for ω_p at peak intensity) of the RFS seeds ($a_\pm\delta\phi_\pm$) for the positive and negative skew pulses from Fig. 4(a) for varying density. This shows a large asymmetry in the RFS seed when $\omega_{p0}\tau_{\mathrm{FWHM}} \sim 10$. Also shown in Fig. 4(b) is the maximum amplitude of the seed $[a_+\delta\phi_+(\zeta)]_{\max}$ which decreases with increasing density or pulse duration; i.e., for large density or pulse duration, the pulse envelope contribution to seeding RFS is small.

In the experiment for case 1, the laser is at high intensity throughout the whole plasma: It enters at high intensity and then relativistic guiding keeps it focused. As the pulse encounters the low density plasma in the front of the jet profile, the fast rise time is able to excite large plasma waves when $\omega_{p0}\tau_{\mathrm{FWHM}} \sim 10$, resulting in a larger seed. For slow rise times, the response is weaker and lower amplitude plasma waves ensue. The asymmetry in

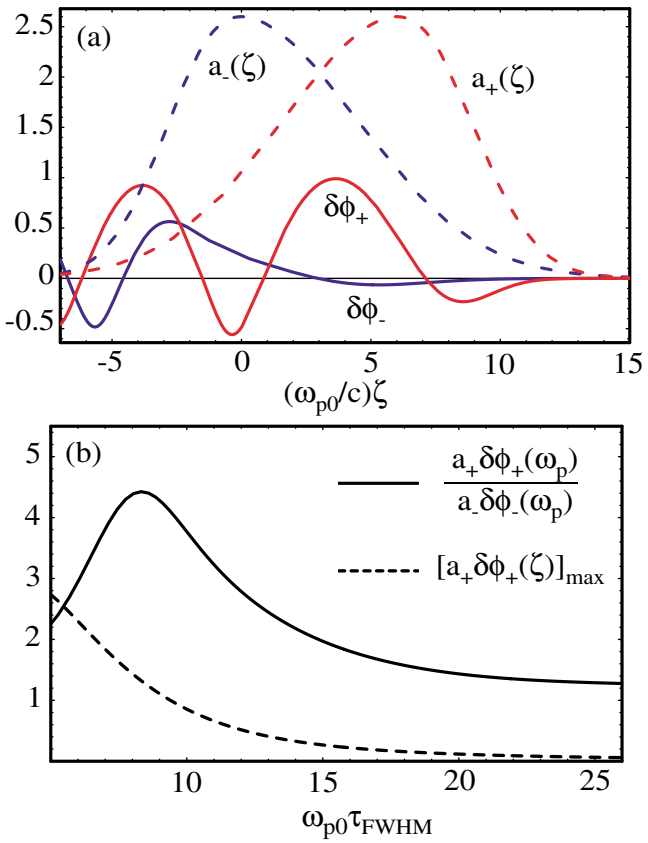

FIG. 4 (color). (a) Plasma wave potential $\delta\phi_{\pm}$ (solid curves) excited by pulse envelope $a_{\pm}(\zeta)$ (dashed curves) for positive (red curves) and negative (blue curves) skewed pulses with $\omega_{p0}\tau_{\mathrm{FWHM}} = 6$ for $2 \times 10^{18}\ \mathrm{cm}^{-3}$ density (gas jet ramp). (b) The solid curve is the ratio of the Fourier components (evaluated for ω_p at peak intensity) of the RFS seeds ($a_{\pm}\delta\phi_{\pm}$) with pulse shapes of (a), as a function of density. Dashed curve is the maximum of $[a_{+}\delta\phi_{+}(\zeta)]$.

redshifted sidebands observed in the experiment is also consistent with enhanced RFS for fast rise times.

When the laser pulse was focused deeper into the jet (case 2), before the pulse reaches high intensity, it has traversed much of the lower density gas at lower intensity. As can be seen in Fig. 4(b), in the high density region, where $\omega_{p0}\tau_{\mathrm{FWHM}} \gtrsim 20$, seeding of the plasma wave due to envelope effects is much less sensitive to pulse asymmetries. Furthermore, on the ramp, the lower laser pulse intensity results in smaller plasma wave amplitudes and again smaller seeds. The maximum wave amplitude (electron yield) then occurs for shorter laser pulses, i.e., near the normal compressor zero. Note that ionization induced refraction and blueshifting may cause some steepening of the pulse, independent of chirp, and therefore mask any chirp induced asymmetries.

Simulations (1D) with XOOPIC qualitatively confirmed these results. A fast rising pulse propagating up a ramp followed by a flat density region yielded ~3 times more electrons with energy > 15 MeV than for a gentle rising pulse. However, when starting the pulse on the flat region the number of electrons was nearly identical.

In conclusion, experiments have demonstrated for the first time that optimization and significant enhancement of laser driven accelerators can be accomplished using properly shaped laser pulse envelopes. Electron yields can be produced with fast rising pulses which in some cases are nearly an order of magnitude larger than for slow rising pulses. The effect of envelope asymmetry on enhancement of RFS and self-modulation is found to be much more important than that of linear chirp in pulses with symmetric (e.g., Gaussian) temporal envelopes.

We acknowledge the contributions of L. Archambault, K. Barat, D. Bruhwiler, G. Brussaard, J. Cary, M. Dickinson, D. Dimitrov, G. Dugan, S. DiMaggio, G. Fubiani, and R. Short. We acknowledge H.-J. Lee and J. Wurtele for developing 1D XOOPIC. This work was supported by DOE Contract No. DE-AC-03-76SF0098. C. Geddes acknowledges the Hertz Foundation.

*Also at Technische Universiteit Eindhoven, the Netherlands.

[1] E. Esarey *et al.*, IEEE Trans. Plasma Sci. **24**, 252 (1996).
[2] W. L. Kruer, *The Physics of Laser-Plasma Interactions* (Addison-Wesley, Redwood City, CA, 1988).
[3] G. Laval *et al.*, Phys. Fluids **20**, 2049 (1977).
[4] E. S. Dodd and D. Umstadter, Phys. Plasmas **8**, 3531 (2001).
[5] A. Modena *et al.*, Nature (London) **377**, 606 (1995).
[6] D. Umstadter *et al.*, Science **273**, 472 (1996).
[7] A. Ting *et al.*, Phys. Plasmas **4**, 1889 (1997).
[8] W. P. Leemans *et al.*, Phys. Plasmas **8**, 2510 (2001).
[9] J. Faure *et al.*, Phys. Rev. E **63**, 065401 (2001).
[10] V. I. Berezhiani and I. G. Murusidze, Phys. Scr. **45**, 87 (1992).
[11] J. Krall *et al.*, Phys. Plasmas **1**, 1738 (1994).
[12] M. D. Perry and G. Mourou, Science **264**, 917 (1994).
[13] Cs. Toth *et al.*, in Advanced Acceleration Concepts, 2002, edited by C. Clayton and P. Muggli, AIP Proceedings (AIP, New York, to be published).
[14] E. Esarey *et al.*, IEEE J. Quantum Electron. **33**, 1879 (1997).
[15] W. M. Wood, C. W. Siders, and M. C. Downer, Phys. Rev. Lett. **67**, 3523 (1991).
[16] E. Esarey, G. Joyce, and P. Sprangle, Phys. Rev. A **44**, 3908 (1991).
[17] W. P. Leemans *et al.*, Phys. Rev. A **46**, 1091 (1992).
[18] C. B. Schroeder *et al.*, Phys. Plasmas (to be published).
[19] E. Esarey *et al.*, Phys. Rev. Lett. **80**, 5552 (1998).
[20] T. M. Antonsen, Jr. and P. Mora, Phys. Rev. Lett. **69**, 2204 (1992).
[21] W. B. Mori *et al.*, Phys. Rev. Lett. **72**, 1482 (1994).
[22] W. B. Mori, IEEE J. Quantum Electron. **33**, 1942 (1997).
[23] J. P. Verboncoeur, A. B. Langdon, and N. T. Gladd, Comput. Phys. Commun. **87**, 199 (1995).